Cellular/Molecular

Ca^{2+} Sparks and Puffs Are Generated and Interact in Rat Hippocampal CA1 Pyramidal Neuron Dendrites

Kenichi Miyazaki[1,2] **and William N. Ross**[1,2]

[1]Department of Physiology, New York Medical College, Valhalla, New York 10595, and [2]Marine Biological Laboratory, Woods Hole, Massachusetts 02543

1,4,5-Inositol trisphosphate receptors (IP_3Rs) and ryanodine receptors (RyRs) mediate release of Ca^{2+} from internal stores in many neurons. The details of the spatial and temporal characteristics of these signals and their interactions in dendrites remain to be clarified. We found that localized Ca^{2+} release events, with no associated change in membrane potential, occurred spontaneously in the dendrites of rat hippocampal CA1 pyramidal neurons. Their rate, but not their amplitude or time course, could be modulated by changes in membrane potential. Together, these results suggest that the spontaneous events are similar to RyR-dependent Ca^{2+} "sparks" found in cardiac myocytes. In addition, we found that we could generate another kind of localized Ca^{2+} release event by either a synaptic tetanus in the presence of 3-((*R*)-2-carboxypiperazine-4-yl)-propyl-1-phosphonic acid and CNQX or by uncaging IP_3. These events had slower rise times and decay times than sparks and were more heterogeneous. These properties are similar to Ca^{2+} "puffs" found in oocytes. These two localized signals interact. Low-intensity tetanic synaptic stimulation or uncaging of IP_3 increased the decay time of spontaneous Ca^{2+} events without changing their rise time or amplitude. Pharmacological experiments suggest that this event widening is attributable to a delayed IP_3R-mediated release of Ca^{2+} triggered by the synergistic action of IP_3 and Ca^{2+} released by RyRs. The actions of IP_3 appear to be confined to the main apical dendrite because uncaging IP_3 in the oblique dendrites has no effect on the time course of localized events or backpropagating action potential-evoked Ca^{2+} signals in this region.

Introduction

The most studied sources of postsynaptic $[Ca^{2+}]_i$ changes in hippocampal pyramidal neurons are Ca^{2+} entry through NMDA receptors in dendritic spines and Ca^{2+} entry through voltage-gated Ca^{2+} channels, opened primarily by backpropagating action potentials (bAPs). Because these $[Ca^{2+}]_i$ changes appear to be important in the induction of some forms of synaptic plasticity and other signaling cascades, there has been intense interest in understanding these signals.

Less attention has been devoted to the details of $[Ca^{2+}]_i$ changes resulting from Ca^{2+} release from internal stores, possibly because they are not as closely linked to changes in membrane potential. It is generally recognized that, in many cell types, Ca^{2+} can be released through two different channels on the endoplasmic reticulum (ER): (1) ryanodine receptors (RyRs); and (2) 1,4,5-inositol trisphosphate receptors (IP_3Rs; Berridge, 1998). However, especially in neurons, there is sparse information about where release from these receptors occurs and how these signals interact with other Ca^{2+} signaling processes. Synaptically activated Ca^{2+} release has been detected in the dendrites of Purkinje neurons and several kinds of pyramidal neurons, and localized Ca^{2+} release events have been detected in presynaptic terminals and cell bodies (Pozzo-Miller et al., 1996; Nakamura et al., 1999; Conti et al., 2004; ZhuGe et al., 2006; for review, see Ross, 2012).

Previously (Manita and Ross, 2009), we reported that spontaneous, localized Ca^{2+} release events occur in dendrites of hippocampal pyramidal neurons and other neurons in the CNS. We noted that they had some features in common with Ca^{2+} "sparks" described in cardiac myocytes and other preparations (Cheng and Lederer, 2008), in which RyRs are abundant and modulation by IP_3 rarely occurs. They also have features in common with Ca^{2+} "puffs" described in *Xenopus* oocytes and other cells (Parker and Ivorra, 1990) in which IP_3Rs are abundant and RyRs are absent (Parys et al., 1992). Immunocytochemical experiments indicate that IP_3R (type 1) and RyR (type 1) are both present in hippocampal CA1 pyramidal neurons (Hertle and Yeckel, 2007). However, it is not clear whether these localized events reflect two distinct mechanisms of Ca^{2+} release or whether they reflect only one process, which can be activated in different ways. To answer this question, we used high-speed Ca^{2+} imaging to look for distinguishing characteristics of these events, particularly their kinetics. These experiments showed that both sparks and puffs can be generated separately in the dendrites. We also found that these two mechanisms can interact. We found that synaptically evoked mGluR activation, acting through the generation of IP_3, increased the decay time of spontaneous spark Ca^{2+} transients without affecting spark rise times or peak amplitudes. This IP_3-dependent process also locally increased the decay time of Ca^{2+} transients evoked by bAPs. Both of these increases in decay time were attributable to the delayed release of Ca^{2+}

Received June 27, 2013; revised Sept. 16, 2013; accepted Oct. 3, 2013.

Author contributions: K.M. and W.N.R. designed research; K.M. performed research; K.M. and W.N.R. analyzed data; K.M. and W.N.R. wrote the paper.

This work was supported in part by National Institutes of Health Grant NS016295. We thank Nechama Ross for computer programming.

The authors declare no competing financial interests.

Correspondence should be addressed to Dr. William Ross, Department of Physiology, New York Medical College, Valhalla, NY 10595. E-mail: ross@nymc.edu.

DOI:10.1523/JNEUROSCI.2735-13.2013

 0270-6474/13/3317777-12$15.00/0

triggered by the synergistic interaction of Ca^{2+} and IP_3 acting on the IP_3R to release more Ca^{2+}. The initial source of Ca^{2+} was either a spark or a bAP. Interestingly, both Ca^{2+} puffs and IP_3-dependent spark modulation occurred only on the main apical dendrites; there were no IP_3-mediated changes on the oblique dendrites, although some spark-like events could be detected in that region.

Materials and Methods

Whole-cell recording and stimulation. Transverse hippocampal slices (300 μm thick) from Sprague Dawley rats (P8–P15, either sex) were prepared as described previously (Manita and Ross, 2009; Miyazaki et al., 2012). Animals were anesthetized with isoflurane and decapitated using procedures approved by the Institutional Animal Care and Use Committees of New York Medical College and the Marine Biological Laboratory. Slices were cut in an ice-cold solution of artificial CSF (ACSF) composed of the following (mM): 80 NaCl, 2.5 KCl, 0.29 $CaCl_2$, 7 $MgCl_2$, 1.25 NaH_2PO_4, 25 $NaHCO_3$, 75 sucrose, 10.1 glucose, 1.3 ascorbate, and 3 pyruvate. They were incubated for at least 1 h in solution consisting of the following (mM): 124 NaCl, 2.5 KCl, 2 $CaCl_2$, 2 $MgCl_2$, 1.25 NaH_2PO_4, 26 $NaHCO_3$, 10.1 glucose, 1.3 ascorbate, and 3 pyruvate making the final pH 7.4 (bubbled with a mixture of 95% O_2–5% CO_2). Normal ACSF (in mM: 124 NaCl, 2.5 KCl, 2 $CaCl_2$, 2 $MgCl_2$, 1.25 NaH_2PO_4, 26 $NaHCO_3$, and 10.1 glucose) was used for recording.

Submerged slices were placed in a chamber mounted on a stage rigidly bolted to an air table and were viewed with a 60× water-immersion lens in an Olympus BX50WI microscope mounted on an *x–y* translation stage. Somatic whole-cell recordings were made using patch pipettes pulled from 1.5-mm-outer-diameter thick-walled glass tubing (1511-M; Friedrich and Dimmock). Tight seals on CA1 pyramidal cell somata were made with the "blow and seal" technique using video-enhanced differential interference contrast optics to visualize the cells (Stuart et al., 1993). For most experiments, the pipette solution contained the following (in mM): 130 potassium gluconate, 4 NaCl, 4 Mg-ATP, 0.3 Na-GTP, 7 Na-phosphocreatine, and 10 HEPES, pH adjusted to 7.3 with KOH. Final osmolarity was 290 mOsm. This solution was supplemented (except when noted) with 50 μM Oregon Green BAPTA-1 (OGB-1; a high-affinity calcium indicator; Invitrogen) and, in some experiments, 100–200 μM caged IP_3 (Invitrogen or EMD4Biosciences). We usually waited 30 min after membrane rupture before starting measurements. Temperature in the chamber was maintained between 29 and 33°C.

Dynamic $[Ca^{2+}]_i$ measurements. Time-dependent $[Ca^{2+}]_i$ measurements from different regions of the pyramidal neuron were made as described previously (Lasser-Ross et al., 1991; Manita and Ross, 2009). We used a RedShirtImaging NeuroCCD-SMQ camera, controlled by their Neuroplex software. The camera has 80 × 80 pixels and was read out at 500 Hz. A custom program (SCAN) was used to analyze and display the data. We measured fluorescence changes of OGB-1 with excitation at 494 ± 10 nm and emission at 536 ± 20 nm. The light source was a 75 W xenon arc lamp, whose output intensity was often reduced to 25% with a neutral density filter. In most experiments, we used an Olympus 60×, 1.1 numerical aperture lens to maximize the detected light. $[Ca^{2+}]_i$ changes are approximated as $\Delta F/F$, where F is the fluorescence intensity when the cell is at rest and ΔF is the change in fluorescence during activity. In some cases, corrections were made for indicator bleaching during trials with sparks and spikes by subtracting a linear fit to the signal measured under the same conditions when the cell was not stimulated, after normalizing the unstimulated trace to the same value at the start of the trial, i.e., every point in the unstimulated trace was mul-

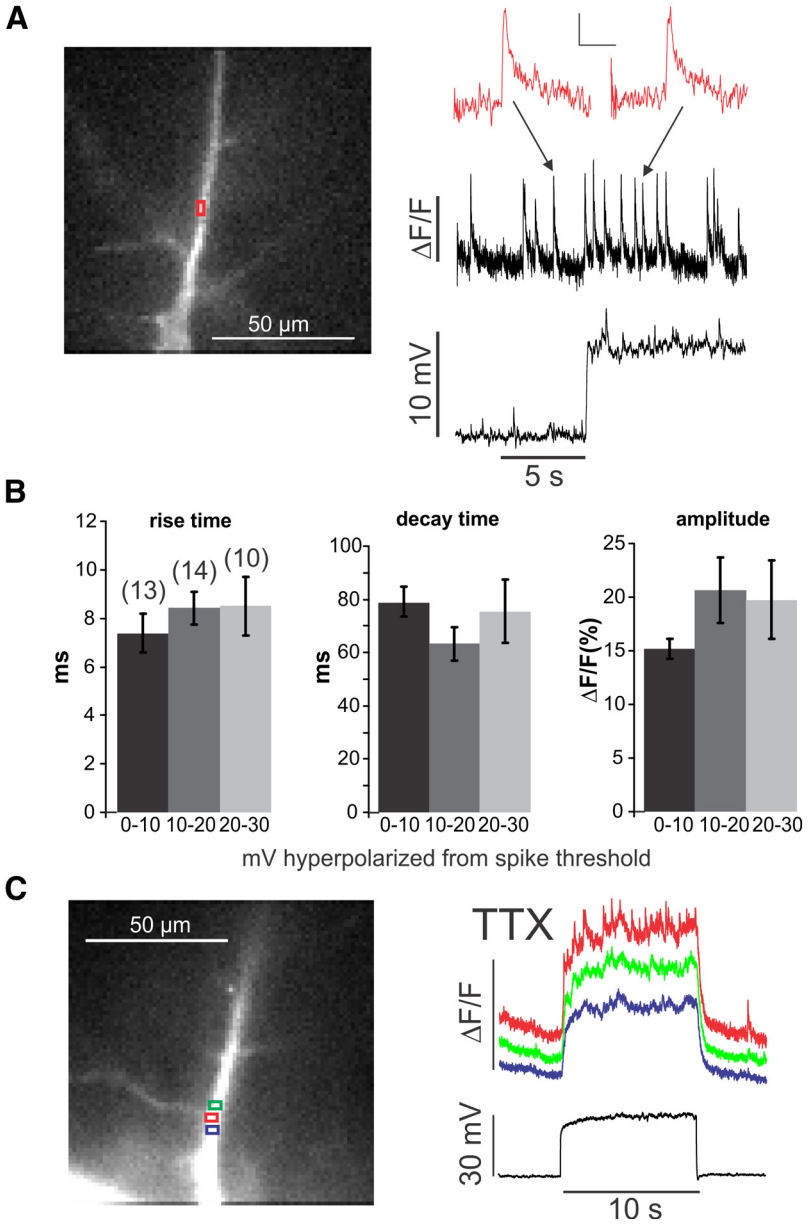

Figure 1. Changing membrane potential increases the frequency of spontaneous sparks but does not change their kinetic parameters or change them into propagating events. ***A***, Spontaneous events detected at a dendritic location (red ROI). The fluorescence image shows a pyramidal neuron filled with OGB-1. During the 10 s trial, the membrane potential was depolarized by 10 mV, increasing the rate of events. The inset shows two events, one before and one after the depolarization. There was no change in the kinetics or amplitude. Calibration: inset, $\Delta F/F$, 200 ms. ***B***, Histograms of rise times (10–90%), half-decay times, and amplitudes of spontaneous events measured at different potentials below the threshold for spike generation. There were no significant changes ($p > 0.3$ in all cases). Numbers in parentheses above bars are numbers of measured events, same for all three histograms. ***C***, $[Ca^{2+}]_i$ changes measured at three neighboring locations in the dendrites in response to a 30 mV step depolarization in ACSF containing 1 μM TTX. The rate of events increased at the center location (red trace) but did not change at the neighboring sites. The steady increase in $[Ca^{2+}]_i$ at all three sites was attributable to voltage-dependent Ca^{2+} entry.

tiplied by the ratio of the mean of the *F* values for the first five sampled points (10 ms) of the two traces. In these neurons, when we used the 60× lens, we could examine $[Ca^{2+}]_i$ increases over a range of 93 μm with the NeuroCCD-SMQ camera. Increases in different parts of the cell are displayed using either selected regions of interest (ROIs) or a pseudo "line-scan" display (Nakamura et al., 2000).

In a typical experiment, we patched a CA1 pyramidal neuron on the soma and allowed 30 min for OGB-1 and caged IP_3 to diffuse into the dendrites. We focused on the dendrites, typically positioning the soma just outside the field of illumination to reduce photodynamic damage. To examine the spatial distribution of postsynaptic $[Ca^{2+}]_i$ changes, we selected pyramidal neurons that were in the plane of the slice and close to the surface. In our conditions, we recorded at least five (usually 10) trials of 20 s duration before signs of photodynamic damage.

Photolysis of caged IP_3. Caged IP_3 was allowed to diffuse throughout the cell after membrane rupture. Pulsed UV light centered at 365 nm from a light-emitting diode (UVILED; Rapp Optoelectronics) entered the microscope through a side port via a 200-μm-diameter quartz fiber optic light guide. It was reflected off a 420 nm dichroic mirror (allowing transmission of the 488 nm excitation light) and was focused through the objective, making a spot of ~10 μm in diameter on the slice with the 60× objective lens. UV light intensity was regulated by changing the fraction of time the UV light was on during a high-frequency pulse train (Manita and Ross, 2010).

Measurement of spark and puff parameters. In some of the experiments, we measured the rise times, decay times, spatial extents, and amplitudes of localized Ca^{2+} release events. All of these parameters can be distorted by indicator buffering, the kinetics of the Ca^{2+}: indicator reaction, the frame rate of the camera, the size and position of the ROIs, and the filtering algorithms used to improve the signal-to-noise ratio (S/N). The main concern was to achieve sufficient accuracy to distinguish puffs from sparks. To this end, we found that using 50 μM OGB-1, together with running the camera at 500 Hz, introduced minimal distortion of the rise time and decay time (Miyazaki et al., 2012). To improve the S/N, we sometimes temporally filtered the traces with either a 7-point or an 11-point weighted smoothing algorithm. We used the smallest ROI possible to make quantitative measurements (usually a single pixel, covering an area of 1.16 × 1.16 μm^2) and positioned it to give the largest event amplitude. In most cases (see Results), these choices were sufficient to distinguish puffs from sparks. The weakest measurement was event amplitude because there is likely a steep spatial gradient even within the small ROIs. Error bars in the figures are SEM except when noted.

Results

Characteristics of spontaneous events

We recorded from apical dendrites of CA1 pyramidal cells filled with 50 μM OGB-1. We observed the dynamic $[Ca^{2+}]_i$ level in the dendrites during a 20 s trial without synaptic stimulation. As shown previously (Manita and Ross, 2009), we detected brief Ca^{2+} transients in the dendrites that were not associated with any changes in membrane potential (Fig. 1*A*). They appeared at many different locations and at stochastic intervals. Typical event rise times (10–90%) and half-decay times (time-to-decay to half-peak amplitude) were 7.8 ± 0.6 and 67 ± 4.2 ms (n = 45; selected at random from hundreds). However, these times depended on the age of the animal, becoming faster as they matured (Miyazaki et al., 2012). They appeared to come from a source of 1–2 μm length and spread by diffusion over a slightly wider spatial extent (Manita and Ross, 2009; Miyazaki et al., 2012; see Fig. 3*D*).

The frequency of these spontaneous events could be affected by changes in membrane potential in the subthreshold range (Manita and Ross, 2009). This modulation could be prevented by L-type Ca^{2+} channel blockers (nifedipine and nimodipine) and enhanced by Bay K-8644 (1,4-dihydro-2,6-dimethyl-5-nitro-4-[2-(trifluoromethyl)phenyl]-3-pyridinecarboxylic acid, methyl

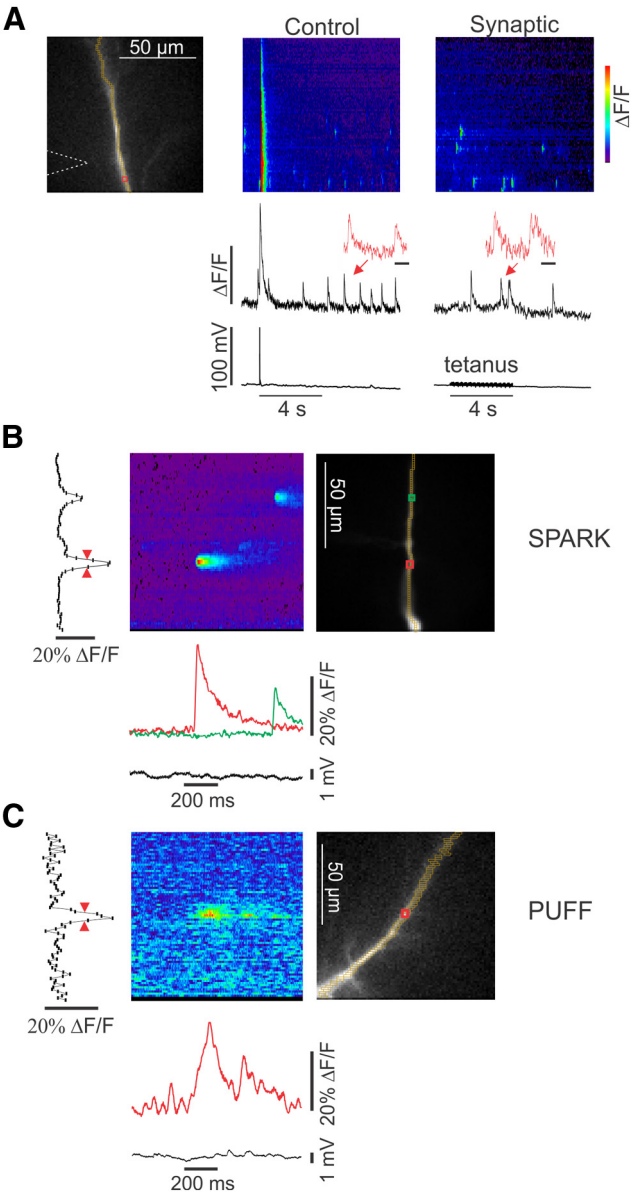

Figure 2. Characteristics of spontaneous localized events and synaptically evoked events in the dendrites. ***A***, The image shows a dendrite with an ROI and the location of the stimulating electrode marked. The "Control" frame shows a line scan along the dendrite and the signals at the ROI. The response to a stimulated bAP and spontaneous events are shown. The inset shows two of the events at higher speed. The "Synaptic" frame shows the response to a 4 s, 100 Hz synaptic tetanus in the presence of 10 μM CNQX, 10 μM 3-((*R*)-2-carboxypiperazine-4-yl)-propyl-1-phosphonic acid, and 100 μM picrotoxin. The inset shows that some of the events during the tetanus appear to be slower than the spontaneous events. Calibration: insets, 200 ms. ***B***, Detail of two spontaneous events (sparks). Both have fast rise time and decay times. The amplitude scan at the left shows the maximum $\Delta F/F$ during the time window of the trace for each pixel. The width (red arrows) is ~4 μm. Each pixel is 1.16 μm. ***C***, Detail of an event (puff) generated by IP_3 uncaging. This event had a slower rise time and a width of ~6 μm.

ester), indicating that the role of the L-type channels was to allow voltage-dependent Ca^{2+} entry. In the new experiments (Fig. 1), we characterized this modulation in more detail. We found that the voltage-dependent frequency increase occurred without any significant change in the rise time, decay time, or amplitude of the events (Fig. 1*B*). The voltage-dependent rate increase never led to a regenerative propagating Ca^{2+} wave even with a strong depolarization in the presence of TTX (Fig. 1*C*). In addition, the spontaneous events were not blocked by intracellular heparin, a

nonspecific IP_3R blocker (1–5 mg/ml, $n = 9$ cells; Ghosh et al., 1988), although this concentration clearly reduced IP_3-dependent Ca^{2+} waves (Nakamura et al., 1999; Manita and Ross, 2009). All these observations are consistent with the conclusion that the spontaneous events are generally constant in their kinetic parameters and similar to RyR-dependent sparks in myocytes (Cheng and Lederer, 2008). A diagram suggesting how these isolated sparks are generated is shown in Figure 8*A*.

mGluR- and IP_3-mediated events and signal modulation

Previously, we showed that strong repetitive synaptic stimulation in the presence of APV and CNQX evoked large-amplitude Ca^{2+} waves (Nakamura et al., 1999), and weaker repetitive stimulation increased the frequency of localized events (Manita and Ross, 2009). Similar Ca^{2+} waves and localized events were generated by uncaging IP_3 in the dendrites, supporting the conclusion that the synaptically stimulated events were generated by mGluR mobilization of IP_3 (Manita and Ross, 2009, 2010). In new experiments, we looked more carefully at the events evoked during repetitive synaptic stimulation, comparing their properties with those of spontaneous events described above. Figure 2*A* shows that some events (arrows) appeared to have longer durations during the tetanus compared with events at other times. We recorded many events with these characteristics, but it was difficult to quantitatively assess the changes because we did not know clearly whether the presynaptic fibers innervated the dendritic region in which the events occurred or whether the mGluRs were responding throughout the 4 s tetanus (see Fig. 7*E*,*F*). To overcome this limitation, we used focal uncaging of IP_3, which allowed us to control the time, duration, and location of IP_3 generation. The amount of released IP_3, determined by the intensity of the UV flash, was selected to be below the threshold for evoking a regenerative Ca^{2+} wave. We quantitatively examined the parameters of a random subset of these uncaged events. In this analysis, we found it useful to divide them into two groups. The first group contained events that occurred at locations in the dendrites in which we did not detect spontaneous events before stimulation; we defined these events as puffs. The second group included events at locations in which spontaneous events did occur in resting conditions.

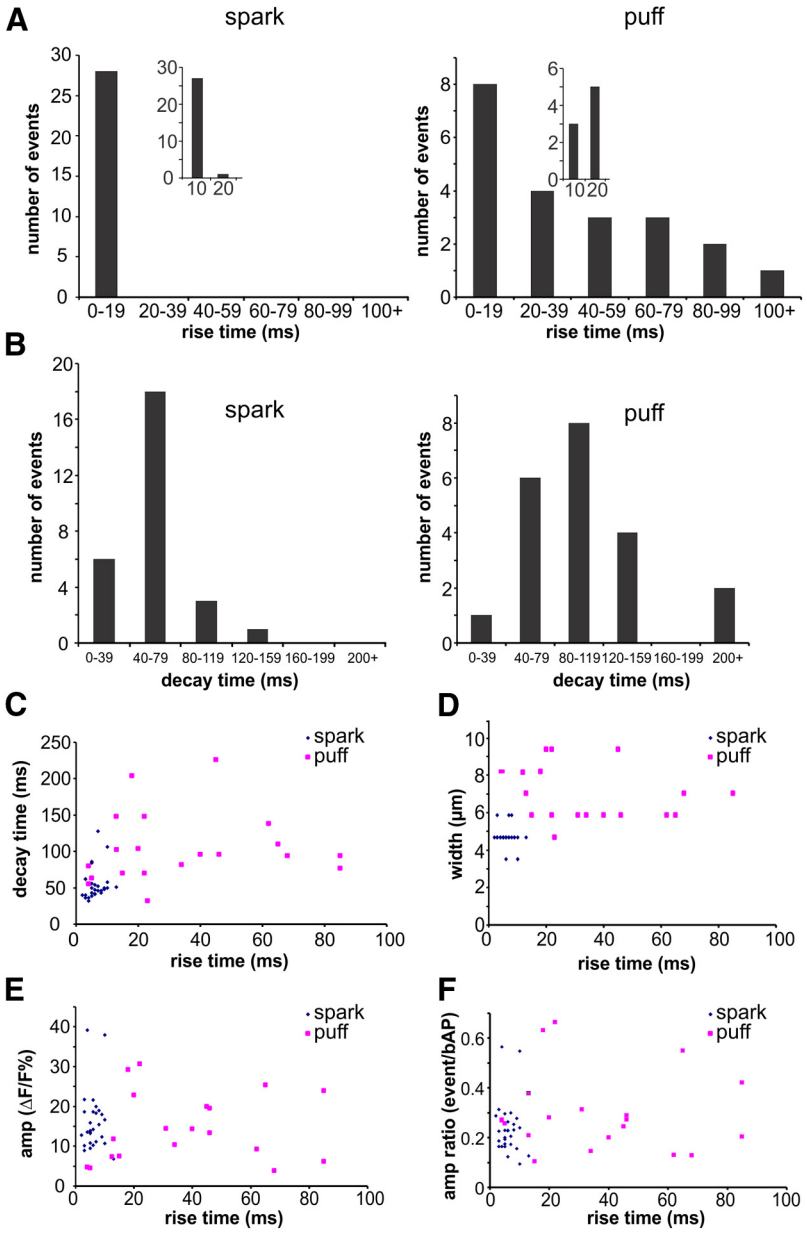

Figure 3. Comparison of event parameters for sparks and puffs. ***A***, Histograms of rise times (10–90%) for sparks and puffs. The insets show the first 20 ms bin divided into two parts. All sparks had fast rise times, most under 10 ms. Puff rise times ranged between 4 and 100 ms, with only three events faster than 10 ms. ***B***, Histograms of half-decay times for sparks and puffs. Puffs had slower decay times than sparks, but the difference was not as strong as the difference in rise times. ***C***, Scatter plot of rise and decay times of sparks and puffs. Puffs were slower and more heterogeneous than sparks. There was no clear correlation between the rise and decay times for either event type. ***D***, Scatter plot of event width and rise time. Puffs were wider, but there was no clear correlation between width and rise time. ***E***, Scatter plot of event amplitude and rise time. There was no clear difference in amplitude between sparks and puffs and no clear correlation between amplitude and rise time for either event type. ***F***, Scatter plot of event amplitudes, normalized to the amplitude of a bAP signal at the same locations, versus rise time.

The first group was heterogeneous. They were generally slower than the spontaneous sparks (Fig. 2*B*,*C*). They had rise times that ranged from 4 to 200 ms and decay times that ranged from 50 to 200 ms (Fig. 3*A*,*B*). It is possible that a few of the fastest events were really spontaneous events (sparks) that occurred during the time of uncaging but were absent at other examined times, but only 3 of 21 measured puffs fell into this category. The spatial extent of the puffs was also variable, although the apparent width (which reflects Ca^{2+} diffusion as well as the size of the source) of most events (~7 μm) was larger than the extent of most spontaneous events (Fig. 3*D*). There was no correlation between the rise time and spatial extent of puffs (Fig. 3*D*). Because the decay time of the rapidly rising sparks is determined by Ca^{2+} diffusion and membrane pumps (Miyazaki et al., 2012), the slower decay times of these stimulated events probably indicates sustained Ca^{2+} release on the falling phase of the events,

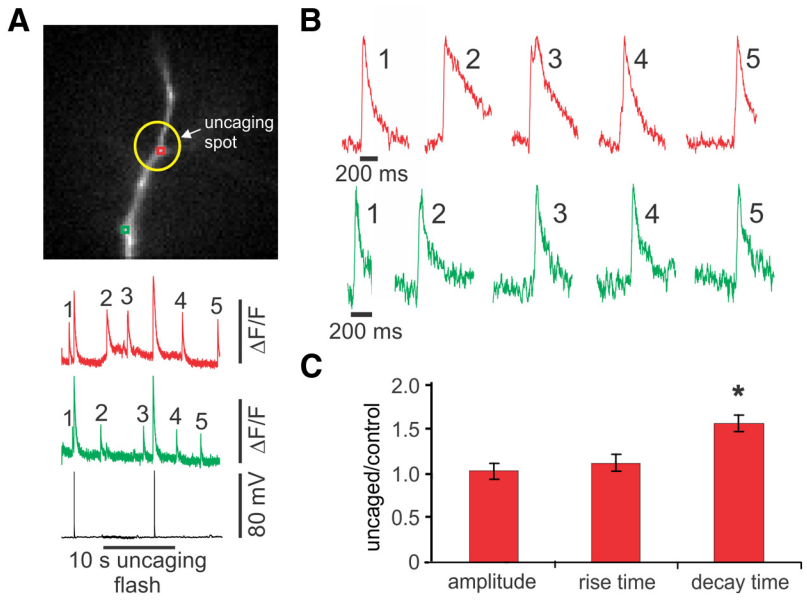

Figure 4. Focal uncaging of IP_3 in the dendrites widens sparks at the site of uncaging without affecting their rise times or amplitude. ***A***, Image of dendrite with two ROIs and the site of uncaging (yellow circle). During the 20 s trace, IP_3 was uncaged for 10 s. Responses to two bAPs and spontaneous events were recorded. ***B***, At the site of uncaging (red traces), the apparent decay time of the events increased compared with the decay times of events outside the uncaging time. There was no clear change at the site away from the uncaging (green trace). ***C***, Histograms of the ratio of amplitudes, rise times, and decay times of the first two events occurring during the uncaging pulse and inside the uncaging location to the average of these parameters before the uncaging pulse. Only the decay times changed significantly ($n = 15$ pairs, each pair an average of 2 events of each kind; $^*p < 0.001$, paired *t* test).

a greater spatial extent of the source, or both (Miyazaki et al., 2012). They were still faster than the decay times of bAP signals, which have no component because of Ca^{2+} diffusion (Miyazaki et al., 2012). The traces during uncaging were usually noisier than the traces examined in the analysis of spontaneous events, so it was more difficult to measure the amplitudes accurately. Nevertheless, we found no major difference between the size of the spontaneous sparks and the size of the stimulated puffs (Fig. 3*E*). Most of the puff signals were 10–60% as large as the signals from bAPs at the same location (Fig. 3*F*). This heterogeneity in kinetics and size are similar to the properties of IP_3-dependent puffs detected in oocytes (Sun et al., 1998).

The events in the second group affected by uncaging were longer lasting than the spontaneous sparks detected at the same locations in the dendrites. In these experiments, we locally uncaged IP_3 for 10 s during a 20 s trial. Several events occurred both within the uncaging region (yellow circle) and outside this region (Fig. 4*A*). The expanded traces (Fig. 4*B*) show that the events within the uncaging region (especially the earlier events; see Fig. 7) had longer decay times than those outside this zone. On average (Fig. 4*C*), the half decay times of events generated in the presence of elevated IP_3 were ~50% greater than events outside this region. Additional analysis showed that the decay time was the only event parameter affected by uncaging; neither the rise time nor the amplitude was significantly changed (Fig. 4*C*).

We suspected that the increased event decay time (after either a synaptic tetanus or an uncaging flash) was attributable to increased Ca^{2+} release through IP_3Rs during the falling phase of the events. However, it was difficult to reliably detect events within the zone of synaptic activation (unknown) or the uncaging region. Therefore, we tested the effect of an mGluR-mediated synaptic tetanus and IP_3 uncaging on bAP-evoked Ca^{2+} signals. bAPs can be reliably evoked by brief intrasomatic depolarization, and the $[Ca^{2+}]_i$ changes they generate are spread over most of the dendritic field (Jaffe et al., 1992). Previously, we found that stimulating a bAP during a synaptic tetanus (Nakamura et al., 1999) or in the presence of uncaged IP_3 (Manita and Ross, 2010) generated a Ca^{2+} wave. However, if we reduced the intensity of the tetanus (Fig. 5*A*,*B*) or UV flash (Fig. 5*C*), we found that a typical bAP-associated Ca^{2+} signal was generated in the dendrites except that the apparent decay time of the signal was increased. This widening was graded; increasing the intensity of the UV uncaging flash increased the extent of widening (Fig. 5*D*). Using strong synaptic stimulation or higher UV flash energy than shown in this figure evoked fully regenerative Ca^{2+} waves (Nakamura et al., 1999; Manita and Ross, 2010; data not shown). (Although increasing the intensity of the synaptic tetanus and increasing the intensity of the UV flash produced similar results, we note that the increased production of IP_3 was achieved in a slightly different manner. Increasing the intensity of the UV flash increases the production of IP_3 similarly at all locations in the targeted region. Increasing the synaptic stimulation intensity recruits more presynaptic fibers targeting a larger area; each activated fiber presumably mobilizes the same amount of IP_3, independent of the stimulation intensity.) The widening of the bAP-evoked Ca^{2+} signal occurred only in the region that was targeted by the tetanus or uncaging (Fig. 6*C*) and occurred only during the time of stimulation or uncaging. Because there was no widening in the region distal to the activated region (Fig. 5*A*), the widening could not be attributable to a change in the electrical parameters of the bAPs in the stimulated region because this would have affected electrical propagation into the distal region. In addition, there was no change in the somatically recorded AP (data not shown). These results suggest that the widening of bAP-evoked Ca^{2+} transients and the widening of Ca^{2+} sparks occurred through the same mechanism.

Pharmacology of event and spike signal widening

Because the bAP-evoked $[Ca^{2+}]_i$ change resulted from Ca^{2+} entry through voltage-gated Ca^{2+} channels, it was easier to test whether the widening of the bAP-evoked Ca^{2+} signal was attributable to Ca^{2+} release from stores. Figure 6 shows that cyclopiazonic acid (CPA), a blocker of the sarcoplasmic Ca^{2+}-ATPase (SERCA) pump, which leads to store depletion (Seidler et al., 1989), prevented the widening of bAP Ca^{2+} signals evoked by uncaging IP_3, similar to the way CPA prevented the generation of bAP-evoked Ca^{2+} waves (Nakamura et al., 1999, 2000). At the same time, CPA widened the bAP-evoked Ca^{2+} transient in control conditions (because one of the pumps was eliminated) as shown previously (Sabatini et al., 2002). Together, these experiments suggest that the widening of localized event Ca^{2+} signals and the widening of bAP-evoked Ca^{2+} signals are both attributable to the release of Ca^{2+} from the ER on the falling phase of the signal. We could not test the effect of CPA on the widening of

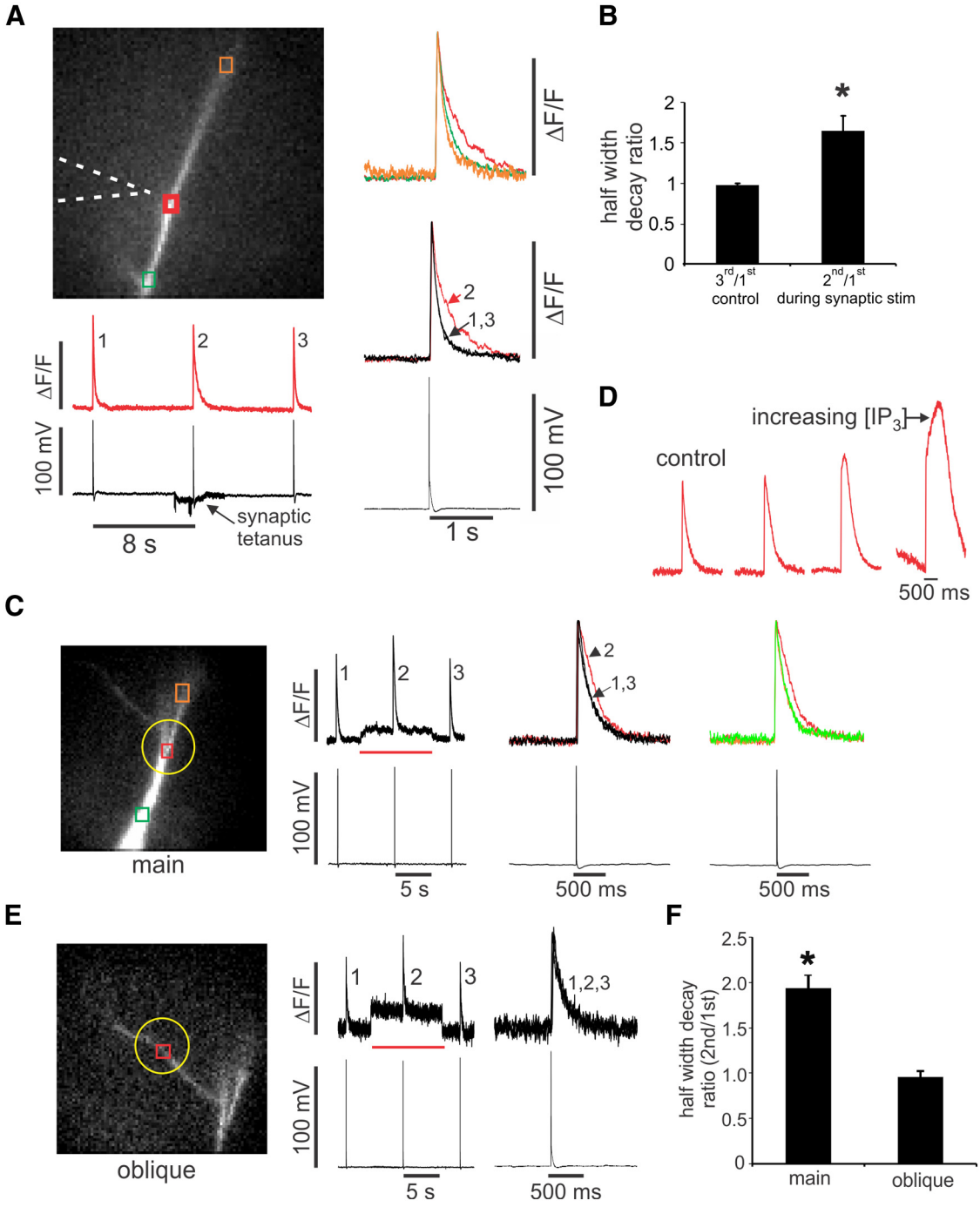

Figure 5. Synaptic stimulation or focal IP_3 uncaging locally increases the decay time of bAP-evoked Ca^{2+} signals on the main apical dendrite but not on the oblique branches. ***A***, Three bAPs were evoked at 8 s intervals. A 4 s tetanus (100 Hz) in the presence of 10 μM CNQX, 10 μM 3-((*R*)-2-carboxypiperazine-4-yl)-propyl-1-phosphonic acid, and 100 μM picrotoxin was stimulated at the time of the second bAP. The traces to the right show that the decay time of the second spike signal, but not the first or third, was increased but only at the site opposite the stimulating electrode. ***B***, Summary histogram shows this result for five cells ($*p < 0.02$). ***C***, A similar local widening occurs using caged IP_3 at the time of the second bAP. The uncaging pulse lasted 10 s (red bar). Most of the steady increase in $\Delta F/F$ during this time is an artifact from incomplete blockage of the UV light from the fluorescence pathway. ***D***, Responses at the uncaging site to increasing concentration of IP_3, regulated by increasing the intensity of the UV flash. The responses are graded, with greater decay times in response to higher IP_3 levels. At even higher levels (data not shown), a regenerative Ca^{2+} wave was evoked. ***E***, A similar experiment with the uncaging pulse over the oblique dendrite of the same cell as in Figure 5*C*. There was no change in the bAP-evoked Ca^{2+} signal decay time. ***F***, Summary histogram showing that there was a significant change only on the main dendrite ($n = 5$; $*p < 0.005$).

spark signals because CPA blocks sparks (Manita and Ross, 2009).

Previously (Manita and Ross, 2009), we examined the effects of several putative blockers of RyRs and IP_3Rs on spontaneous Ca^{2+} release events. At that time, we did not distinguish between sparks and puffs, which complicated the interpretation of some experiments. The reduction of spark frequency by dantrolene, an RyR blocker (Hainaut and Desmedt, 1974), and the enhancement of spark frequency by caffeine support the interpretation of sparks as RyR-dependent events. However, dantrolene also had an effect on Ca^{2+} waves, which suggested caution in interpretation of those results. In new experiments, we

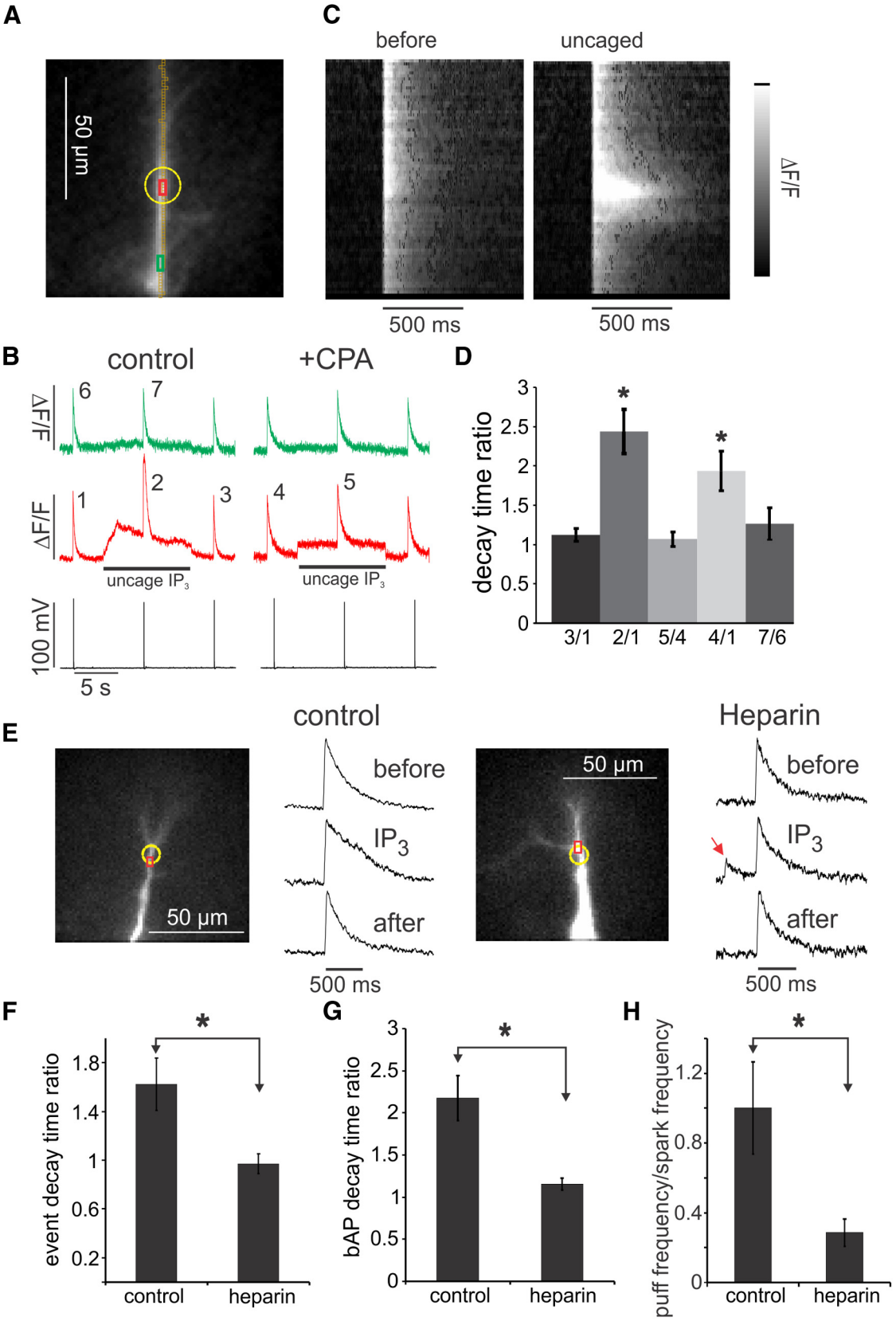

Figure 6. CPA and heparin block IP_3-mediated widening of bAP signals and heparin blocks spark widening. ***A***, The image shows two ROIs, the site of IP_3 uncaging (yellow circle), and the set of pixels for the line scan. ***B***, Ca^{2+} transients in response to bAPs in control conditions and in the presence of 20 μM CPA while focally uncaging IP_3. Outside of the uncaging spot (green traces), the time courses of all three transients are the same in normal ACSF and all three are widened in CPA. Inside the uncaging spot (red traces), the transient is wider in the presence of uncaged IP_3 in normal ACSF (transient 2 compared with transient 1). At the end of the uncaging pulse, the transient returns to the original decay time (transient 3 compared with transient 1). However, uncaging does not increase the decay time more than CPA does alone (transient 5 compared with transient 4). ***C***, The grayscale images show the line-scan presentation of bAP-evoked $[Ca^{2+}]_i$ changes along the dendrite. The first image ("before," corresponding to signal 1 in ***B***) shows that the transient is approximately constant along the dendrite in control conditions. (*Figure legend continues.*)

revisited the interpretation of some results and tested some additional potential blockers. We found that tetracaine did not eliminate sparks or affect puffs, even at a concentration of 500 μM in the pipette, although it reduces spark frequency in muscle fibers predominantly by reducing the amplitude of the Ca^{2+} source flux (Hollingworth et al., 2006). We found that xestospongin C, a putative IP_3R blocker (Gafni et al., 1997) included in the patch pipette (at concentrations up to 10 μM), did not block spontaneous sparks or affect the generation of caged IP_3-induced puffs, bAP signal widening, or Ca^{2+} waves ($n = 6$ cells). However, the interpretation of this result is not clear because other experiments (De Smet et al., 1999; Castonguay and Robitaille, 2002; Solovyova et al., 2002) suggest that the main effect of this compound really is to block SERCA and membrane pumps with little effect on IP_3Rs.

We found that the nonspecific IP_3R blocker heparin (5 mg/ml in the pipette) did selectively reduce puff frequency (Fig. 6*H*) and blocked IP_3-dependent bAP signal and spark widening without eliminating sparks (Fig. 6*E–G*). In comparing cells with and without heparin, we were careful to use the same concentration of caged IP_3 and the same intensity of the UV flash in paired cells from the same slice. Furthermore, doubling the UV intensity in heparin-loaded cells did not lead to Ca^{2+} waves or puffs, whereas lower intensity often generated Ca^{2+} waves in cells without heparin. These results are consistent with our interpretation that puffs are IP_3R-dependent events.

During a long IP_3 uncaging pulse, it appeared that the widening of the events was greater in the earlier part of the stimulus (Fig. 4*B*). Analyzing similar trials in many cells showed that this was a common trend (Fig. 7*A*). However, the width of the first event during the UV pulse was widened by approximately the same amount no matter when it occurred compared with controls before the pulse, although there was a lot of scatter in the data (Fig. 7*B*). The decrease in event widening could be attributable to adaptation or desensitization in some step of the signaling cascade or to a reduction in the amount of IP_3 generated during the long UV pulse. To distinguish among these possibilities, we compared the response to three bAPs separated by 4 s during the uncaging pulse. Figure 7, *C* (top) and *D*, shows that the width of the third bAP signal was significantly narrower than the width of the first bAP signal. However, when only one bAP was evoked at the time of the last bAP in the three-spike trial, the width of this signal was not significantly different from the width of the first bAP signal (Fig. 7*C*, bottom, *D*). This suggests that IP_3 was generated at approximately a constant level throughout the long UV pulse. In a series of similar experiments, using a long synaptic tetanus instead of a long UV pulse, we found that only the first bAP signal was significantly wider than control signals (Fig. 7*E*, top, *F*). Also, in the case when only a single trial was evoked at the end of the tetanus, there was no widening (Fig. 7*E*, bottom, and *F*). This shows that, unlike during the uncaging pulse, IP_3 is not produced continuously during the synaptic tetanus, probably because of a reduction in presynaptic spike-evoked glutamate release during the tetanus. The similarity of the adaptation of the spark signals and bAP signals during the long uncaging pulse suggests that they both occur by the same mechanism. Two possibilities are inactivation of IP_3Rs (Marchant and Taylor, 1998) and local depletion of the stores releasing Ca^{2+}.

Signals on oblique dendrites

All of these results relate primarily to events located on the primary apical dendrites of CA1 pyramidal neurons. The main reason for this selection is that this region was easiest to observe because slices could, with practice, be cut with this dendrite in the plane of the slice and close to the surface. Oblique dendrites project in unpredictable directions from the apical shaft. A second reason for this selection is that we observed previously (Nakamura et al., 2002; Larkum et al., 2003) that Ca^{2+} waves were most prominent on the main dendrite with little Ca^{2+} release on the obliques. Therefore, we wanted to restrict our initial analysis to a region that might have relatively homogeneous properties. However, we were able to detect some events on oblique dendrites (Manita and Ross, 2009; confirmed in these new experiments), although at lower frequency than on the main shaft. We did not quantify this conclusion because several factors (e.g., dendritic caliber, level of indicator filling, and extent of dendritic region in focus) differed between the main shaft and obliques, making comparisons difficult. Nevertheless, we could measure the effect of IP_3 uncaging on event parameters and spike signals in both dendritic regions. Interestingly, we found that uncaging IP_3 did not widen the bAP signals in this region (Fig. 5*E*,*F*). We do not think this result is attributable to a lack of sensitivity in the obliques because, in many experiments, we used twice the usual concentration of OGB-1 (100 μM) and waited at least 30 min for the indicator and caged IP_3 to diffuse to these processes. We also tested the effect of caged IP_3 on the time course of spontaneous events on the oblique dendrites. Unfortunately, we were only able to test the effect on three cells. We found that there was no change in decay time, consistent with the effect on the bAP-evoked signals. However, it is clear that more work is needed to analyze events on the obliques.

Discussion

Sparks and puffs are distinct events

A primary result of these experiments is the clear distinction between two types of localized Ca^{2+} release events in pyramidal neuron dendrites. One kind, similar to sparks in myocytes and other preparations, is mediated by RyRs. They occur spontaneously, have fast (<10 ms) rise times, and decay rapidly by a combination of diffusion and membrane pumps (Miyazaki et al., 2012). Their frequency can be modulated by changes in membrane potential, but their other measureable parameters (rise time, decay time, and amplitude) are insensitive to voltage. Even when their frequency is dramatically increased by strong depolarization, they do not coalesce into regenerative Ca^{2+} waves that spread beyond their initiation site. The other kind of event, similar to puffs in oocytes, rarely

←

(*Figure legend continued.*) The second image ("uncaged," corresponding to signal 2 in ***B***) shows that the decay time of the transient increased in the uncaging zone. There does not appear to be any spatial heterogeneity in this region. ***D***, Summary histograms showing these results for six cells. Only the ratios of transients 2/1 and 4/1 were significantly different from 1 (*$p < 0.02$). ***E***, Response to three successive bAPs at 8 s intervals in control cells and in cells with 5 mg/ml heparin. A 10 s uncaging pulse (yellow circle) surrounded the second bAP in each trial. Uncaging IP_3 did not widen the bAP signal in the heparin-filled cell. However, spontaneous sparks still occurred (red arrow). ***F***, Summary statistics showing no spark widening in heparin-loaded cells compared with control cells ($n = 5$ cells; *$p < 0.05$). ***G***, Summary statistics showing no widening of bAP signals in cells with heparin compared with control cells (5 mg/ml) in the pipette ($n = 5$ cells; *$p < 0.05$). ***H***, Ratio of puffs (events with rise times >15 ms) to sparks (events with rise times <15 ms) detected in the uncaging region on the dendrites in cells with normal internal solution plus caged IP_3 (100 μM) and in cells containing caged IP_3 and heparin (5 mg/ml). Fifty-eight events were examined in control conditions and 76 events in cells with heparin. There was a significantly smaller fraction of puffs in heparin-loaded cells (*$p < 0.01$). Errors bars are SD. Paired *t* test used in ***F–H***.

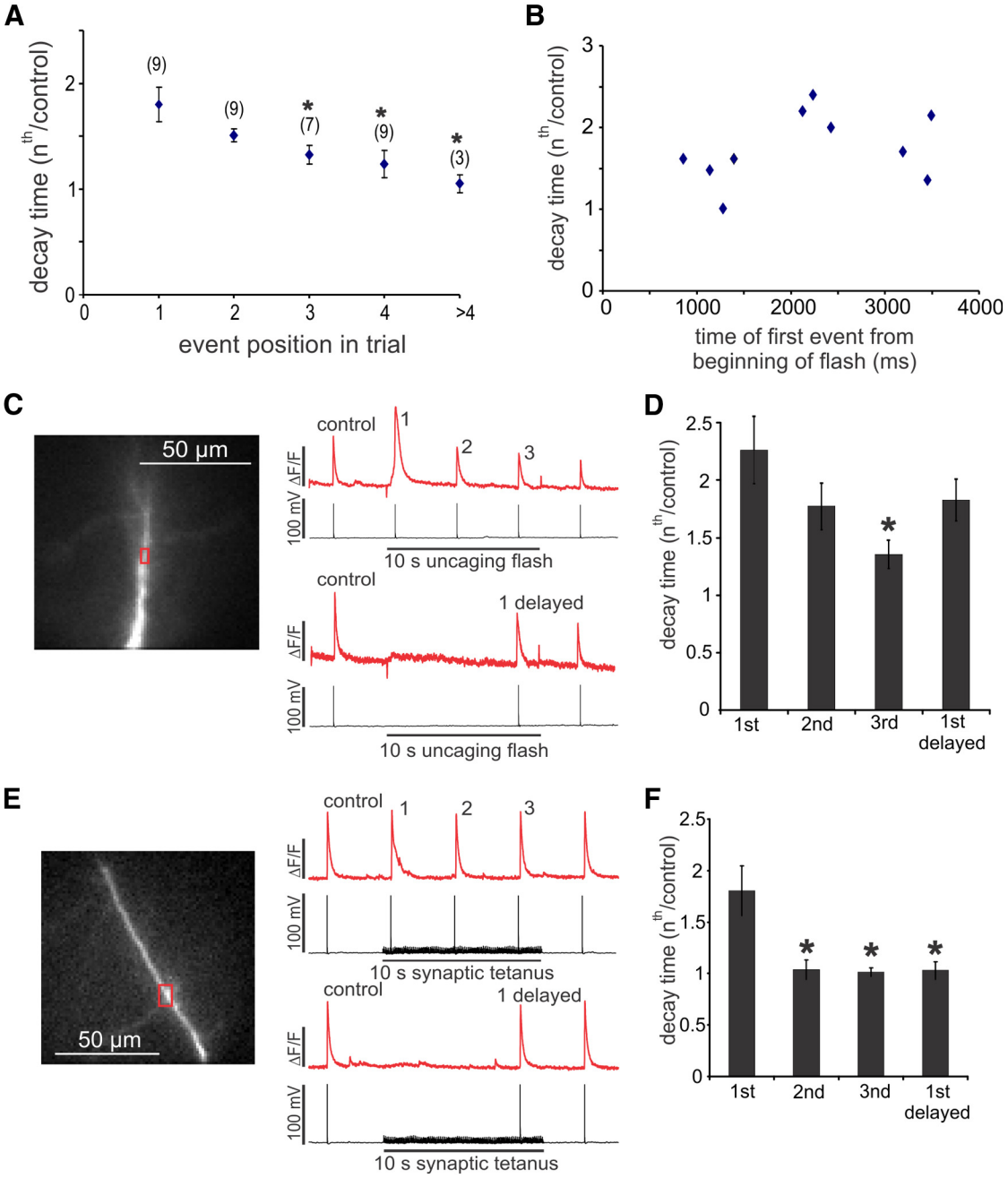

Figure 7. Spark width adaptation during a long uncaging pulse is not attributable to a reduction in available IP_3. ***A***, Summary histogram of many experiments like the one in Figure 4 showing that the decay times of successive events during a flash get faster. The third and later events are significantly faster than the first event ($*p < 0.05$). Decay times are compared with the average decay time of several events before the flash. Numbers in parentheses are number of events. ***B***, Decay time of the first event detected during a long uncaging pulse compared with the average decay time of several events before the flash. There does not appear to be a change, although there was considerable heterogeneity in the responses. ***C***, Top red trace, Response to five successive bAPs, three occurring during a 10 s uncaging flash. The later responses were smaller and faster than the first response. Bottom red trace, Response to three bAPs, with the middle one delayed to the end of the flash. The response was similar to the first undelayed response. ***D***, Summary histogram comparing decay times of bAP signals during the uncaging flash with the decay time of a bAP signal before the uncaging flash for eight cells. Only the third signal was significantly different from the first trace ($*p < 0.05$). Because the delayed signal is similar to the first signal, IP_3 was probably available throughout the UV flash. ***E***, Similar experiment using a 10 s tetanus (100 Hz) instead of a 10 s uncaging pulse. The top red trace shows that the first transient was wider than the later transients. However, when the first bAP was delayed (bottom red trace), the transient was not wider. ***F***, Summary histogram of data from five cells. All the later decay times are significantly faster than the first one ($*p < 0.05$).

occurs spontaneously. It is mediated by IP_3Rs, usually after IP_3 mobilization by synaptic activation of mGluRs. Their rise times and decay times are slower than those of sparks and are more heterogeneous. Their frequency is increased by higher levels of IP_3, and they easily coalesce into Ca^{2+} waves. These properties are similar to those found in oocytes (Callamaras et al., 1998; Sun et al., 1998). Figure 8, *B* and *C*, shows a model of how this transition occurs. The heparin experiments, blocking puffs and spark widening but not sparks, reinforce the distinction between these two kinds of release events. The more stereotypical pattern of sparks may reflect a more constant size of the RyR clusters that produce the sparks than the more heterogeneous clusters of IP_3Rs that underlie puffs in other preparations (Sun et al., 1998; Cheng and Lederer, 2008). Also, not all IP_3Rs in a cluster may be acti-

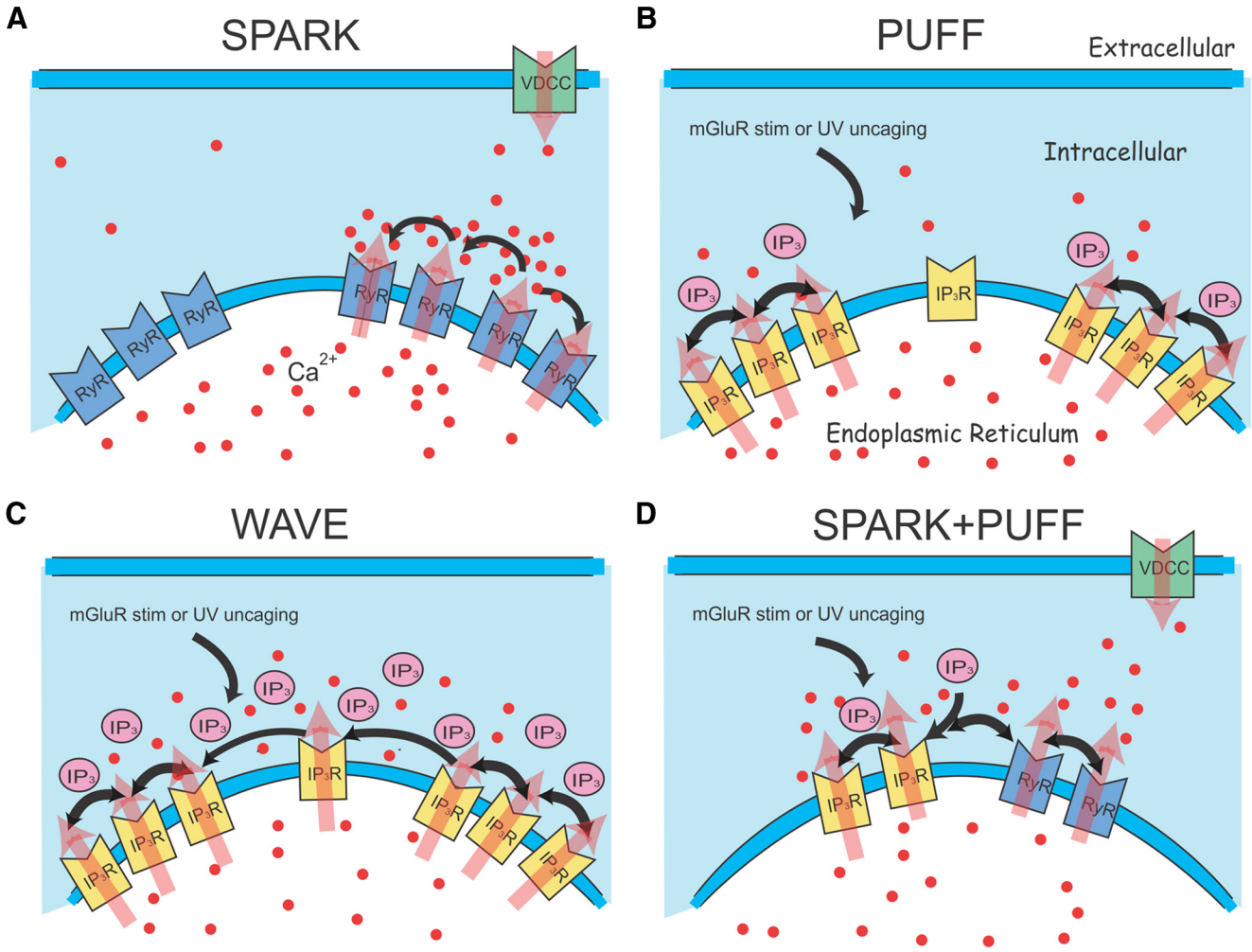

Figure 8. Simple models of how sparks, puffs, waves, and spark–puff interactions are generated in the dendrites. ***A***, Sparks occur by local CICR among a cluster of RyRs. Their rate can be enhanced by Ca^{2+} entry through L-type Ca^{2+} channels. Because sparks do not propagate, we assume that clusters are far enough apart so Ca^{2+} from one cluster does not affect another. ***B***, ***C***, Puffs and waves can be generated from the same set of IP_3Rs. If the level of IP_3 (generated by mGluR stimulation or uncaging) is low, then only a few IP_3Rs in each cluster are opened and the resulting CICR is not strong enough to activate nearby clusters resulting in a puff. With higher levels of IP_3, more IP_3Rs are opened and CICR spreads to nearby IP_3R clusters and leads to a wave. In both these cases, we assume that the resting $[Ca^{2+}]_i$ level is sufficient to act as a cofactor opening some IP_3Rs. ***D***, If a cluster of RyRs is near a cluster of IP_3Rs, then Ca^{2+} released from a spark can activate more IP_3Rs in the nearby cluster than the resting $[Ca^{2+}]_i$ level can in the presence of some IP_3. Ca^{2+} released from the IP_3Rs appears on the falling phase of the spark because IP_3R openings are usually slower than RyR openings.

vated by Ca^{2+}-induced Ca^{2+} release (CICR) because binding of IP_3 to the receptors is also required.

Although there are two kinds of events, the release of Ca^{2+} from IP_3Rs can be enhanced at the site of a spark if a spark occurs during the time when IP_3 concentration is raised. This enhancement is probably attributable to the fact that the IP_3R requires both Ca^{2+} and IP_3 to open the channel (Bezprozvanny et al., 1991; Iino and Endo, 1992); the Ca^{2+} from the spark supplies the additional Ca^{2+} to initiate CICR. For a model of this interaction, see Figure 8*D*. The coincidence activation is similar to the way a bAP triggers a Ca^{2+} wave in the presence of synaptically mobilized IP_3 (Nakamura et al., 1999; Manita and Ross, 2010). In the current experiments, this additional released Ca^{2+} occurs on the falling phase of a spark instead of increasing the spark amplitude. This delayed release is probably related to the fact that puffs generally have a slower rise time than sparks (Shuai et al., 2006; Cheng and Lederer, 2008; Fig. 3*A*), although it is also possible that the IP_3Rs are positioned farther from RyRs than RyRs are positioned with respect to each other. In this case, Ca^{2+} diffusion from RyRs to IP_3Rs would be responsible for the delayed Ca^{2+} release.

Spatial distributions

The spatial distribution of sparks and puffs and their interaction are complicated and not completely understood. Previously (Manita and Ross, 2009), we showed that the spontaneous events (now clearly sparks) occur most frequently at branch points, especially at the site in which secondary (oblique) dendrites emerge from the primary apical dendrite. Similarly, we found that IP_3-dependent Ca^{2+} waves tend to initiate at branch points (Nakamura et al., 2002). This result might suggest that IP_3Rs also are concentrated at branch points. However, another interpretation is that sparks help to initiate Ca^{2+} waves, similar to the way they enhance IP_3-mediated Ca^{2+} release in the current experiments. In this case, preference for wave initiation at branch points would be attributable to the location of RyRs and not IP_3Rs. It also is possible that both RyRs and IP_3Rs could be clustered at branch points. A separate estimation for the distribution of functional

IP_3Rs comes from the experiments in which the release of caged IP_3 increased the decay time of bAP-evoked Ca^{2+} transients. The clear conclusion from these experiments is that the increase occurs on the main apical dendrite and not on the oblique dendrites. There did not appear to be any obvious variation in Ca^{2+} release within the uncaging zone along the apical dendrite even at branch points (Fig. 6*C*, typical of seven examined cells), although Ca^{2+} diffusion and the lack of precision in these measurements might obscure some microheterogeneity in this structure. At a finer resolution than these experiments, we expect some variation in IP_3R density because isolated puffs are generated (Fig. 8*B*,*C*). Hertle and Yeckel (2007) found IP_3Rs all along the apical dendrite, with clustering at branch points, which matches our observations.

Release of caged IP_3 in the oblique dendrites did not increase the decay time of bAP-evoked transients in this region, suggesting that there are few functional IP_3Rs in these processes. This result is consistent with our previous observations (Nakamura et al., 2002; Larkum et al., 2003; Ross, 2012) that Ca^{2+} waves do not initiate in or propagate far into oblique dendrites. This conclusion is paradoxical because most spines are on oblique or basal dendrites (Megías et al., 2001), and mGluRs, which mobilize IP_3, are thought to be particularly (but not exclusively) located at the base of spines (Baude et al., 1993; Lujan et al., 1996).

Spontaneous events, probably sparks, were detected on oblique dendrites but definitely at a lower frequency per unit length than on the main apical dendrites. As noted above, there was no effect of caged IP_3 on spark kinetics in three experiments, consistent with the conclusion that there are few IP_3Rs on the obliques.

Functional consequences

The function of localized Ca^{2+} release events in dendrites, both sparks and puffs, is not known. To be fair, the function of some other sources of elevated postsynaptic $[Ca^{2+}]_i$, such as Ca^{2+} spikes, NMDA spikes, and dendritic Na^+ spikes, is also not clear. The roles of these dendritic spikes have been interpreted more based on their electrical properties than on their Ca^{2+} signaling properties (Gasparini and Magee, 2006; Lavzin et al., 2012; Xu et al., 2012). One direct consequence of Ca^{2+} release events, the activation of localized K^+ conductances, as observed in smooth muscle (Nelson et al., 1995), does not appear significant in pyramidal neuron dendrites; we have not observed any brief hyperpolarizations corresponding to either puffs or sparks. More likely the targets of these events are proteins and/or signaling complexes colocalized with the clusters of the underlying RyRs and IP_3Rs. These have not been identified.

As we noted previously (Manita and Ross, 2009), the frequency of spontaneous events (sparks) can be significantly increased by membrane depolarization in the subthreshold range that might correspond to summating synaptic potentials or "up states." Similarly, puff frequency could be modulated by patterns of synaptic activation that occur *in vivo*, although that is yet to be determined. The modulation of spark decay time by synaptically mobilized IP_3, corresponding to an increase in the total amount of released Ca^{2+}, provides another way for coincident presynaptic and postsynaptic activity to enhance the size of the Ca^{2+} signal. Based on experiments examining the coincidence time window for Ca^{2+} wave generation (Manita and Ross, 2010), we would estimate that the spark should occur within 300 ms of IP_3 generation to enhance Ca^{2+} release. Whether this increased Ca^{2+} leads to a qualitative change in signaling is not known.

Implications for *in vivo* experiments

Sparks and puffs have not yet been detected in *in vivo* imaging experiments. This failure is most likely attributable to the fact that these events are localized, fast, stochastic, and usually smaller than bAP-evoked signals at the same dendritic locations (Miyazaki et al., 2012). It is likely that sparks occur *in vivo* because they occur spontaneously in slices and most aspects of Ca^{2+} signaling in slices have been reproduced in *in vivo* experiments (Waters et al., 2003). Because puffs require synaptic activation to generate IP_3, it is not clear that the stimulation protocol we used to generate puffs in slices matches the pattern of synaptic activation occurring *in vivo*. However, puff generation seems to require only a low level of IP_3 in a localized region of the dendrites. Low levels of IP_3 generation may correspond to the activation of only a few presynaptic fibers, possibly even a single fiber. The initiation of Ca^{2+} waves, which are evoked by a higher and more sustained level of IP_3, usually require the cooperative action of several neighboring fibers (Nakamura et al., 1999). This pattern may not commonly occur *in vivo*. In fact, physiologically evoked Ca^{2+} waves have not been detected *in vivo*, although the $[Ca^{2+}]_i$ increases are large and spread over an extended dendritic region.

Sparks and puffs could be detected during *in vivo* two-photon experiments if the scanning protocol was optimized for detecting these events. Because localized events have been detected in neocortical pyramidal neurons as well as hippocampal cells (Manita and Ross, 2009), these experiments should be possible with current *in vivo* protocols. Scanning repetitively along the main apical dendrite with a system that has high-speed *z*-axis modulation (Göbel et al., 2007) could be an effective approach. To detect the rapid, localized, dendritic spark transients, it may be necessary to use a classic organic indicator such as OGB-1, as used in our experiments. Although there has been remarkable improvement in genetically encoded Ca^{2+} indicators (Akerboom et al., 2012), it is not clear whether the response time of these new indicators is fast enough to detect these small, rapid, and stochastic events (Zhao et al., 2011).

References

Akerboom J, Chen TW, Wardill TJ, Tian L, Marvin JS, Mutlu S, Calderón NC, Esposti F, Borghuis BG, Sun XR, Gordus A, Orger MB, Portugues R, Engert F, Macklin JJ, Filosa A, Aggarwal A, Kerr RA, Takagi R, Kracun S, et al. (2012) Optimization of a GCaMP calcium indicator for neural activity imaging. J Neurosci 32:13819–13840. CrossRef Medline

Baude A, Nusser Z, Roberts JD, Mulvihill E, McIlhinney RA, Somogyi P (1993) The metabotropic glutamate receptor (mGluR1 alpha) is concentrated at perisynaptic membrane of neuronal subpopulations as detected by immunogold reaction. Neuron 11:771–787. CrossRef Medline

Berridge MJ (1998) Neuronal calcium signaling. Neuron 21:13–26. CrossRef Medline

Bezprozvanny I, Watras J, Ehrlich BE (1991) Bell-shaped calcium-response curves of Ins(1,4,5)P_3- and calcium-gated channels from endoplasmic reticulum of cerebellum. Nature 351:751–754. CrossRef Medline

Callamaras N, Marchant JS, Sun XP, Parker I (1998) Activation and coordination of $InsP_3$-mediated elementary Ca^{2+} events during global Ca^{2+} signals in *Xenopus* oocytes. J Physiol 509:81–91. CrossRef Medline

Castonguay A, Robitaille R (2002) Xestospongin C is a potent inhibitor of SERCA at a vertebrate synapse. Cell Calcium 32:39–47. CrossRef Medline

Cheng H, Lederer WJ (2008) Calcium sparks. Physiol Rev 88:1491–1545. CrossRef Medline

Conti R, Tan YP, Llano I (2004) Action potential-evoked and ryanodine-sensitive spontaneous Ca^{2+} transients at the presynaptic terminal of a developing CNS inhibitory synapse. J Neurosci 24:6946–6957. CrossRef Medline

De Smet P, Parys JB, Callewaert G, Weidema AF, Hill E, De Smedt H, Erneux C, Sorrentino V, Missiaen L (1999) Xestospongin C is an equally potent inhibitor of the inositol 1,4,5-trisphosphate receptor and the

endoplasmic-reticulum Ca^{2+} pumps. Cell Calcium 26:9–13. CrossRef Medline

Gafni J, Munsch JA, Lam TH, Catlin MC, Costa LG, Molinski TF, Pessah IN (1997) Xestospongins: potent membrane permeable blockers of the inositol 1,4,5-trisphosphate receptor. Neuron 19:723–733. CrossRef Medline

Gasparini S, Magee JC (2006) State-dependent dendritic computation in hippocampal CA1 pyramidal neurons. J Neurosci 26:2088–2100. CrossRef Medline

Ghosh T, Eis P, Mullaney J, Ebert CL, Gill DL (1988) Competitive, reversible, and potent antagonism of inositol 1, 4, 5-trisphosphate-activated calcium release by heparin. J Biol Chem 263:11075–11079. Medline

Göbel W, Kampa BM, Helmchen F (2007) Imaging cellular network dynamics in three dimensions using fast 3D laser scanning. Nat Methods 4:73–79. CrossRef Medline

Hainaut K, Desmedt JE (1974) Effect of dantrolene sodium on calcium movements in single muscle fibres. Nature 252:728–730. CrossRef Medline

Hertle DN, Yeckel MF (2007) Distribution of inositol-1,4,5-trisphosphate receptor isotypes and ryanodine receptor isotypes during maturation of the rat hippocampus. Neuroscience 150:625–638. CrossRef Medline

Hollingworth S, Chandler WK, Baylor SM (2006) Effects of tetracaine on voltage-activated calcium sparks in frog intact skeletal muscle fibers. J Gen Physiol 127:291–307. CrossRef Medline

Iino M, Endo M (1992) Calcium-dependent immediate feedback control of inositol 1, 4, 5-trisphosphate-induced Ca^{2+} release. Nature 360:76–78. CrossRef Medline

Jaffe DB, Johnston D, Lasser-Ross N, Lisman JE, Miyakawa H, Ross WN (1992) The spread of Na^{+} spikes determines the pattern of dendritic Ca^{2+} entry into hippocampal neurons. Nature 357:244–246. CrossRef Medline

Larkum ME, Watanabe S, Nakamura T, Lasser-Ross N, Ross WN (2003) Synaptically activated Ca^{2+} waves in layer 2/3 and layer 5 rat neocortical pyramidal neurons. J Physiol 549:471–488. CrossRef Medline

Lasser-Ross N, Miyakawa H, Lev-Ram V, Young SR, Ross WN (1991) High time resolution fluorescence imaging with a CCD camera. J Neurosci Methods 36:253–261. CrossRef Medline

Lavzin M, Rapoport S, Polsky A, Garion L, Schiller J (2012) Nonlinear dendritic processing determines angular tuning of barrel cortex neurons in vivo. Nature 490:397–401. CrossRef Medline

Lujan R, Nusser Z, Roberts JD, Shigemoto R, Somogyi P (1996) Perisynaptic location of metabotropic glutamate receptors mGluR1 and mGluR5 on dendrites and dendritic spines in the rat hippocampus. Eur J Neurosci 8:1488–1500. CrossRef Medline

Manita S, Ross WN (2009) Synaptic activation and membrane potential changes modulate the frequency of spontaneous elementary Ca^{2+} release events in the dendrites of pyramidal neurons. J Neurosci 29:7833–7845. CrossRef Medline

Manita S, Ross WN (2010) IP_3 mobilization and diffusion determine the timing window of Ca^{2+} release by synaptic stimulation and a spike in rat CA1 pyramidal cells. Hippocampus 20:524–539. CrossRef Medline

Marchant J, Taylor C (1998) Rapid activation and partial inactivation of inositol trisphosphate receptors by inositol trisphosphate. Biochemistry 2960:11524–11533. CrossRef Medline

Megías M, Emri Z, Freund TF, Gulyás AI (2001) Total number and distribution of inhibitory and excitatory synapses on hippocampal CA1 pyramidal cells. Neurosci 102:527–540. CrossRef Medline

Miyazaki K, Manita S, Ross WN (2012) Developmental profile of localized spontaneous Ca^{2+} release events in the dendrites of rat hippocampal pyramidal neurons. Cell Calcium 52:422–432. CrossRef Medline

Nakamura T, Barbara JG, Nakamura K, Ross WN (1999) Synergistic release of Ca^{2+} from IP_3-sensitive stores evoked by synaptic activation of mGluRs paired with backpropagating action potentials. Neuron 24:727–737. CrossRef Medline

Nakamura T, Nakamura K, Lasser-Ross N, Barbara JG, Sandler VM, Ross WN (2000) Inositol 1, 4, 5-trisphosphate (IP_3)-mediated Ca^{2+} release evoked by metabotropic agonists and backpropagating action potentials in hippocampal CA1 pyramidal neurons. J Neurosci 20:8365–8376. Medline

Nakamura T, Lasser-Ross N, Nakamura K, Ross WN (2002) Spatial segregation and interaction of calcium signalling mechanisms in rat hippocampal CA1 pyramidal neurons. J Physiol 543:465–480. CrossRef Medline

Nelson MT, Cheng H, Rubart M, Santana LF, Bonev AD, Knot HJ, Lederer WJ (1995) Relaxation of arterial smooth muscle by calcium sparks. Science 270:633–637. CrossRef Medline

Parker I, Ivorra I (1990) Localized all-or-none calcium liberation by inositol trisphosphate. Science 250:977–979. CrossRef Medline

Parys JB, Sernett SW, DeLisle S, Snyder PM, Welsh MJ, Campbell KP (1992) Isolation, characterization, and localization of the inositol 1,4,5-trisphosphate receptor protein in *Xenopus laevis* oocytes. J Biol Chem 267:18776–18782. Medline

Pozzo-Miller LD, Petrozzino JJ, Golarai G, Connor JA (1996) Ca^{2+} release from intracellular stores induced by afferent stimulation of CA3 pyramidal neurons in hippocampal slices. J Neurophysiol 76:554–562. Medline

Ross WN (2012) Understanding calcium waves and sparks in central neurons. Nat Rev Neurosci 13:157–168. CrossRef Medline

Sabatini BL, Oertner TG, Svoboda K (2002) The life cycle of Ca^{2+} ions in dendritic spines. Neuron 33:439–452. CrossRef Medline

Seidler NW, Jona I, Vegh M, Martonosi A (1989) Cyclopiazonic acid is a specific inhibitor of the Ca^{2+}-ATPase of sarcoplasmic reticulum. J Biol Chem 264:17816–17823. Medline

Shuai J, Rose HJ, Parker I (2006) The number and spatial distribution of IP_3 receptors underlying calcium puffs in *Xenopus* oocytes. Biophys J 91:4033–4044. CrossRef Medline

Solovyova N, Fernyhough P, Glazner G, Verkhratsky A (2002) Xestospongin C empties the ER calcium store but does not inhibit InsP3-induced Ca^{2+} release in cultured dorsal root ganglia neurons Cell Calcium 32:49–52. CrossRef

Stuart GJ, Dodt HU, Sakmann B (1993) Patch-clamp recordings from the soma and dendrites of neurons in brain slices using infrared video microscopy. Pflugers Arch 423:511–518. CrossRef Medline

Sun XP, Callamaras N, Marchant JS, Parker I (1998) A continuum of $InsP_3$-mediated elementary Ca^{2+} signalling events in *Xenopus* oocytes. J Physiol 509:67–80. CrossRef Medline

Waters J, Larkum M, Sakmann B, Helmchen F (2003) Supralinear Ca^{2+} influx into dendritic tufts of layer 2/3 neocortical pyramidal neurons *in vitro* and *in vivo*. J Neurosci 23:8558–8567. Medline

Xu NL, Harnett MT, Williams SR, Huber D, O'Connor DH, Svoboda K, Magee JC (2012) Nonlinear dendritic integration of sensory and motor input during an active sensing task. Nature 492:247–251. CrossRef Medline

Zhao Y, Araki S, Wu J, Teramoto T, Chang YF, Nakano M, Abdelfattah AS, Fujiwara M, Ishihara T, Nagai T, Campbell RE (2011) An expanded palette of genetically encoded Ca^{2+} indicators. Science 333:1888–1891. CrossRef Medline

ZhuGe R, DeCrescenzo V, Sorrentino V, Lai FA, Tuft RA, Lifshitz LM, Lemos JR, Smith C, Fogarty KE, Walsh JV Jr (2006) Syntillas release Ca^{2+} at a site different from the microdomain where exocytosis occurs in mouse chromaffin cells. Biophys J 90:2027–2037. CrossRef Medline